Evaluation of Gripping Effect on Strain Distribution in Geosynthetics

A. Y. Dayioglu*
Istanbul Technical University, Turkey (yalcinas@itu.edu.tr)
A. H. Aydilek
University of Maryland College Park, MD, US (aydilek@umd.edu)

ABSTRACT: Wide width tensile strength test is widely used to evaluate the stress-strain relationships of geotextiles and to determine the adequate geotextile type during design stage. This test provides useful data about the average strain distribution, however, localized strains due to production defects, seams and punctured zones may affect the mechanical performance of geosynthetic materials and skew test results. Furthermore, the grip type (i.e., hydraulic or roller grip) used in a tensile strength test may influence the measured stresses and strains due to clamping effect. In this study, a number of both punctured and non-punctured geosynthetic specimens were tested to determine strain distributions under wide-with tensile loading using optical flow techniques. Specimens were tested using both roller and pneumatic grips to identify the effects of clamping. A total of 7 optical flow techniques have been utilized to define strain distributions of the geosynthetics samples under tensile loading. The results indicated that optical flow techniques are highly effective in determining the average strain values. Furthermore, the image-based strains could clearly identify the performance of different grip types. No discernible change in strength was observed under the presence of punctures; however, significant localized strains were evident around the punctured area.

Keywords: Geosynthetics, image analyses, optical flow techniques, strain distributions

1 INTRODUCTION

Use of geosynthetics in a wide variety of civil engineering applications is very common. In many applications, design parameters required are strain at failure, deformation modulus and tensile strength. There are two types of tensile tests that can be performed to determine the tensile strength of a geosynthetic material; wide width tensile strength test (ASTM D-4595) and grab tensile test (ASTM D-4632). In particular, wide width tensile strength tests are preferred due to a larger grab width and due to the fact that the provided units are in force/length (Fluet Jr., 1987). The strength properties are defined in this test at certain strains or elongations and those strains or elongations are only calculated by using the uniaxial deformations. For this purpose, the cross-head displacement method is usually employed where the separation distance between two grips are measured during testing (Kutay et al, 2006). However, no information about the local strains developing during the testing can be obtained (Bais-Singh and Goswami, 1996). In addition, no data about the lateral strains can be obtained using this method. The lateral strains play a significant role in the durability and performance of nonwoven geotextiles particularly. Furthermore, strains due to local anomalies such as punctures, seams or other possible defects that might generate during the production stage cannot be measured which might lead to failures or non-conservative engineering designs (Guler et al. 2005).

In order to measure those local or lateral strains, mechanical methods such as extensometers or strain gauges have been utilized in the past, however, their direct contact with the filaments may result in their disruption (Aydilek et al. 2004). In addition, extensometers record the strains within a geotextile specimen based on the distance between two reference points and those values are average and can be obtained only in selected locations (Cetin et al. 2016). Image-based, non-contact techniques using time-lapse photographic images have proved to provide a better understanding of the strain fields present in a geosynthetic specimens (Aydilek et al. 2004, Shinoda and Bathurst 2004). Using such image-based techniques, also called optical flow techniques, a series of digital images of a geosynthetic taken during tensile testing can be analyzed to evaluate the strain fieldsin large specimens.

2 MATERIALS

In this study, two woven geotextiles, GT1 and GT2, and a non-woven geotextile, GT3, were used. The geotextiles were selected among those commonly used in geotechnical construction. Duplicate tests were performed on each geosynthetic type for quality control. The specimen dimensions were selected for the wide-width tensile test in accordance with ASTM D4595. Properties of the geotextiles are given in Table 1.

Table 1. Geotextile properties

Material	Type	Mass/Area (g/m2)	Structure Type	WW Tensile Strength (Ult, MD, kN/m)
GT1	W	570	PP, fibrillated yarn	105.1
GT2	W	250	PP, monofilament	47.4
GT3	NW	278	PP, Needle-punched	NA

W: Woven, NW: Non-woven, PP: polypropylene, WW: wide width, MD: machine direction, NA: not available

3 METHODS

3.1 *Specimen Preparation*

Six specimens were prepared from each geotextile. One of the six specimens was punctured while the others remained intact. All geosynthetics were subjected to wide-width tensile tests using two different types of clamping: hydraulic and roller grips. Duplicate specimens were tested from each type for quality control purposes. A MTS Sintech loading frame equipped with a 66 kN and a 286 kN capacity load cell was used for testing with hydraulic and roller grips, respectively. The selected strain rate was 11% /min for specimens tested in the hydraulic grips, whereas a strain rate of 12% /min were utilized when roller grips were used for clamping. The dimensions of specimens tested with the hydraulic grips were selected as 457 mm by 200 mm. The specimens prepared for roller grips were trimmed to 1828 mm in length and 250 mm in width. The specimen gage length was selected as 381 mm in all tests. Before testing, the self-weight of the lower grip was used to remove any initial slack in the specimens.

3.2 *Image Acquisition*

Before starting the image acquisition, gridlines were drawn on specimen surfaces using paint markers at a 10 mm spacing to maximize the contrast that is necessary for analyses of the digital frames captured to facilitate the block-matching algorithm for the accurate analysis of displacements. The image acquisition rate was determined based on the displacement in terms of pixel counts between successive frames. Generally, the frames were taken at 10 s intervals to achieve sufficient displacement for measurement. The higher acquisition rates may not yield appreciable displacements between the successive frames, and may cause data storage problems during testing. The speed of the testing machine was 1 mm/min in all tests. The image frames were saved onto a hard disk and analyzed for the in-plane displacements from which the strain distributions were obtained. Images were captured using an analog CCD camera with a close focus zoom lens that had a working distance range of 145–330 mm, and a magnification range of 0.063–0.333. The camera was connected to an IMAQ PCI 1408 image acquisition board installed on a personal computer PC. The board was controlled with a LABVIEW generated application. The setup for the image analysis included a 330-mm x 3460-mm workstation platform, a 460-mm vertical post, a 460-mm horizontal arm, a 90°-angle mount, and a 50-mm diameter through-hole focus mechanism. The geosynthetic specimens were illuminated by fiber optic light guides. The image acquisition board produced eight-bit grayscale images 256 gray colors at a resolution of 640 x 480 pixels. The selected region of interest covered an area of approximately 64 mm x 348 mm centered between the jaw grips of the tension machine. Image acquisition setup is provided in Figure 1.

Figure 1: Photo of image acquisition setup (Aydilek et al. 2006)

It is expected that the measurement of localized strains is a function of the scale in which these strains are measured in the image-analysis method. This becomes particularly important when localized slip occurs in the specimen, in which case, small variations in the measurement scale can greatly change the measured strain values. Since the scale of the image-based strain measurement can be varied and made rather small compared to the mechanical methods, there can be a greater difference between the image-based strains and those measured by mechanical methods. In this study, the images were captured at a field-of-view being somewhat larger than the gauge lengths of the extensometer and strain gauges. The main purpose was to obtain an image-based average strain and compare this value to those registered by these two sensors. The results were comparable; however, it is understood that the size of field-of-view may have an effect on the results. A larger field-of-view will result in lower image resolution i.e., quality. The choice of field-of-view for image capturing is the outcome of a tradeoff between obtaining a representative average strain during the test (how valid an average strain over a larger area is) and assessing distribution of local strains. Therefore, the field-of-view adopted herein was chosen after considering this tradeoff. It requires further research and interpretation to analyze the images captured at different resolutions, which may further help to identify the sensitivity of the methodology and its ability to identify significant variations in local strains and their distribution, which is not typically available in the mechanical methods.

3.3 *Optical Flow Algorithm Methods*

In this study, seven optical algorithm techniques were employed to produce a strain field of a specimen subjected to testing. The (1) Lucas and Kanade (1984) approachutilizes a basic optical flow algorithm. Techniques developed by (2) Horn and Schunck (1981), (3) Black and Anadan (1990) provide more advanced baseline techniques. The optical flow technique developed by (4) Brox et al. (2004) approach uses warping and is one of the most commonly used methods for similar applications. Several newer approaches have been developed in recent years, including (5) descriptor matching in variational motion estimation (Brox and Malik, 2010), (6) spline-based bicubic interpolation called Classic++ (Sun et al. 2010), and (7) Classic+NL, a modified version of Classic++by further integrating median filtering (Sun et al. 2010). Detailed explanations about the techniques are given in Cetin et al (2006).

4 RESULTS AND DISCUSSION

The strain predictions of punctured and non-punctured specimens of three geotextiles tested with roller and hydraulic grips using optical flow techniques are given below. All optical flow techniques were conducted on the images of geosynthetics that were captured during the wide-width tensile tests.

Figures 2-4 show the performance of seven optical flow techniques using both punctured and non-punctured specimens for GT1, GT2 and GT3, respectively. In order to analyze the strains for each geosynthetic specimen, measured displacements were plotted against the length of the image. The slope of the best-fit line provides the average axial strains (Kutay et al. 2006).

Figure 2a indicates that average strains of non-punctured GT1 specimen tested in hydraulic grips were higher than the average strains of non-punctured GT1 specimen tested in roller grips except for the average strains calculated with the BA optical flow technique. The average axial strains calculated from all optical flow techniques were not significantly different from each other. The average strain obtained from BA technique for non-punctured GT1 tested in roller springs was much higher than the average strain values obtained from other optical flow techniques.

On the other hand, Figure 2b indicates that average strains of punctured GT1 specimen tested in hydraulic grips were higher than average strains of punctured GT1 specimen tested in roller grips according to the 5 different optical flow techniques. Brox et al (2004) method concluded that the average strain of punctured GT1 specimen tested in roller grips was slightly higher than average strain of punctured GT1 specimen tested in hydraulic grips. The difference between average strains of punctured GT1 tested in hydraulic grips and punctured GT1 tested in roller grips was 0.25% which was not significant (Kutay et al. 2006). Brox and Malik (2010) method-based data also showed that the average strains of punctured GT1 obtained using both roller and hydraulic grips were the same (Figure 2b).

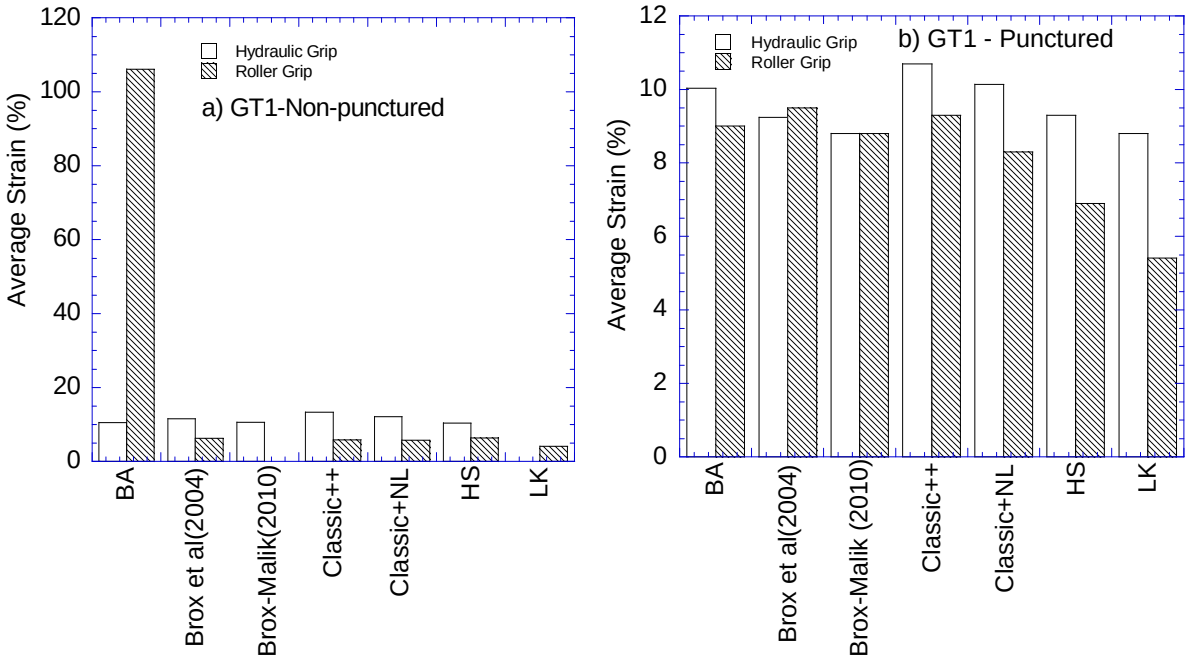

Figure 2: Average strain values using optical flow techniques for a) non-punctured and b) punctured GT1

Average strain values for non-punctured and punctured GT2 specimens are provided in Figure 3(a) and 3(b), respectively. All 7 optical flow techniques provided higher average axial strains for the specimen tested in hydraulic grips than the specimen tested in roller grips. Maximum average strain values between the specimen tested in hydraulic grips and the specimen tested in roller grips was 52%, as recorded by the Brox and Malik (2010) optical flow technique (Figure 3a).

Figure 3b indicates that the average strains of the punctured GT2 specimen tested in roller grips were higher than the average strains of punctured GT2 specimen tested in roller grips based on the calculations made by the BA, Classic++, Classic+NL optical flow techniques. However, HS and LK optical flow techniques provided higher average strain values for the punctured GT2 specimen tested in hydraulic grips. As mentioned in Cetin et al (2016), the Brox and Malik (2010) optical flow technique did not present reasonable strain distributions for the punctured GT2 geosynthetic material. Differences between the average axial strain values for the punctured GT2 specimen were between 2% to 5% with one exception. The difference between average strain of punctured GT2 specimen tested in hydraulic grips than average strain of punctured GT2 specimen tested in roller grips was approximately 16% which was calculated with the HS optical flow technique.

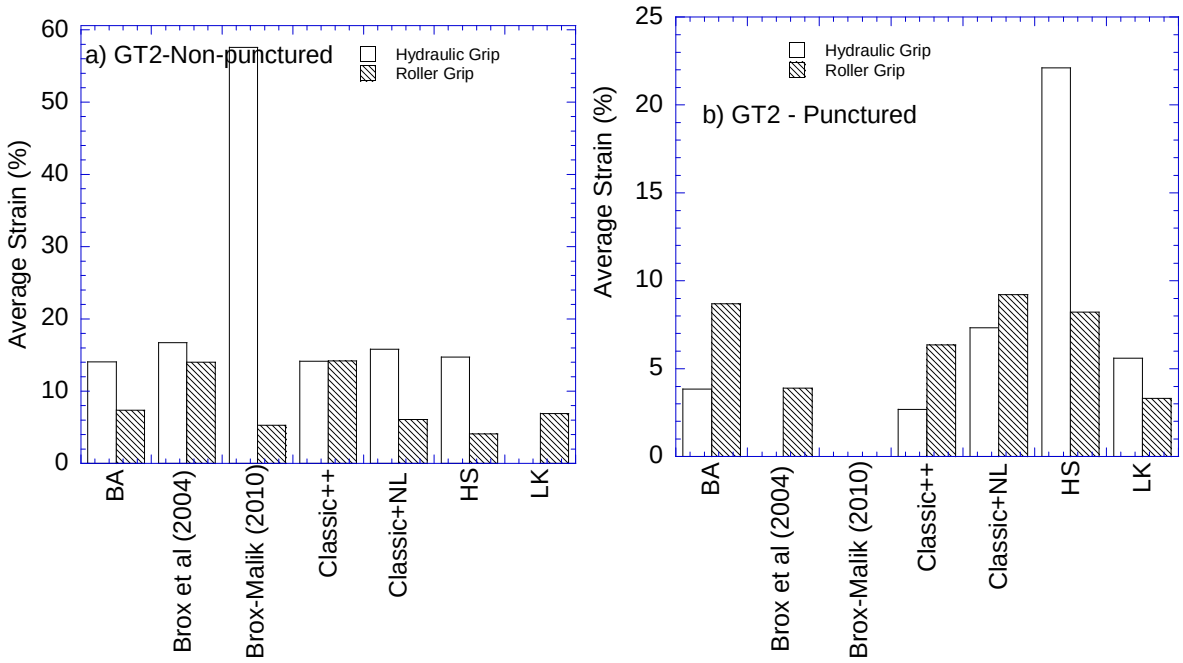

Figure 3: Average strain values using optical flow techniques for a) non-punctured and b) punctured GT2

Based on the results obtained from Figure 4a, the GT3 non-punctured specimen tested in hydraulic grips yielded a higher average axial strain values than the GT3 non-punctured specimen tested in roller grips. The same relationship was observed for all 7 optical flow techniques, particularly for this specimen. However, Figure 4b indicates that punctured GT3 geosynthetic tested in roller springs yielded much higher average axial strain values than punctured GT3 geosynthetic tested in roller springs. The same trend was observed for all 7 optical flow techniques and the differences of average axial strains calculated from GT3 punctured specimen was approximately 15% while this number was not more than 10% for the non-punctured GT3specimen.

Geotextiles are occasionally vulnerable to puncture during field installation. The punctured region may have an effect on the strain distribution of the geosynthetic. These punctured zones may not affect the overall performance of retaining walls or bridge abutments, however, they may cause unexpected failures during capping of soft sediments and sludges especially if the hole diameter is large. In the current study, 8-mm diameter holes were opened on samples of virgin geotextiles per the procedure described in ASTM D 4833 to simulate puncturing occurring in the field (Kutay et al. 2006). Figure 2 shows that the average strain of punctured GT1 is higher than the average strain of non-punctured GT1 if the wide-width tensile test was conducted in hydraulic grips, whereas the average axial strain of non-punctured GT1 tested with roller grips was higher than the average axial strain of the punctured GT1 tested with roller grips. As mentioned in the previous sections, most of the optical flow techniques were not able to provide reasonable strain distributions to simulate field behavior of the GT2 woven geotextile probably due to the larger POA. The data in Figure 4indicates that the average axial strain of GT3 is not significantly affected by the puncture hole at the middle for roller grips. On the other hand, for all the techniques. a sharp decrease was observed in the axial strain values when the test was performed using hydraulic grips.

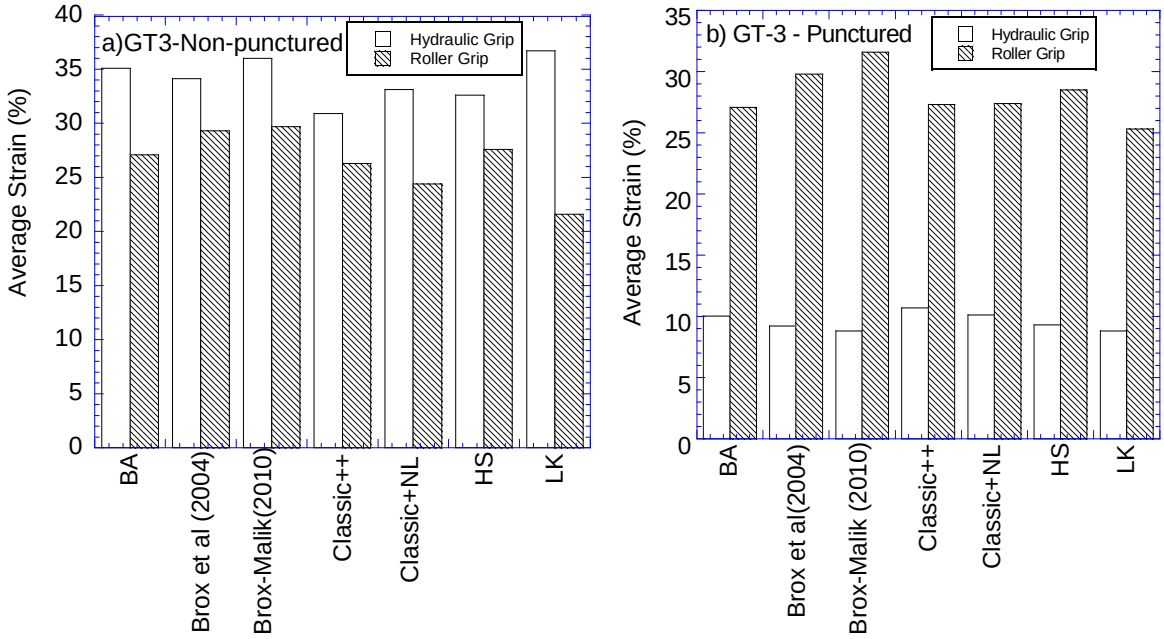

Figure 4: Average strain values using optical flow techniques for a) non-punctured and b) punctured GT3

5 CONCLUSIONS

In this study, three different geosynthetics along with their punctured companions were subjected to wide-width tensile tests using hydraulic and roller grips. Digital images of specimens were captured during testing and analyses of time-lapsed images were performed using seven optical flow techniques to define the strain distributions within the specimen. The observations are summarized as follows:

- The average strain values for non-punctured and punctured specimens of GT1 and GT3 determined using 7 optical flow techniques were very similar to each other of.
- However, the calculated average strains were higher i for GT2, possibly due to its more open monofilament structure (as opposed to fibrillated yarn of GT1)
- The average axial strains appear to be insensitive to puncture when roller grips are used, especially for GT1 and GT3. Most of the optical flow techniques were not able to provide reasonable strain distributions to simulate field behavior of GT2.
- Even though the average axial strain values of GT2 obtained from these optical flow techniques are not so reliable, it can be concluded that axial average strain of GT2 is independent of the puncture effects. However, significant difference is observed when the specimens were tested using hydraulic grips.

ACKNOWLEDGEMENTS

The funding for this project was provided by the Scientific and Technological Research Council of Turkey (TUBITAK). Any opinions, findings, and conclusions or recommendations expressed in this material are those of the authors and do not necessarily reflect the views of TUBITAK.

REFERENCES

ASTM D4595. Standard test method for tensile properties of geotextiles by the wide-width strip method, American Society for Testing and Materials, West Conshohocken, Pennsylvania, USA.

ASTM D4632. Standard Test Method for Grab Breaking Load and Elongation of Geotextiles, American Society for Testing and Materials, West Conshohocken, Pennsylvania, USA.

ASTM STP 952, Fluet, J.E. Jr. (1987). *Geotextile Testing and the Design Engineer*, A Symposium Sponsored by ASTM Committee D-35 on Geotextiles, Geomembranes, and Related Products, Los Angeles, CA, 26 June 1985, Issue 952.

Aydilek, A.H., Guler, M. and Edil, T.B. (2004). Use of image analysis in determination of strain distribution during geosynthetic tensile testing, *Journal of Computational Civil Engineering*, 18(1):65–74.

Bais-Singh, S., and Goswami, B. C. (1996). Deformation behavior of spun-bonded nonwovens: Measurement. *Proceedings of INDA-TEC 96*, Crystal City, Va., 29.1–29.19.

Black, M.J. and Anandan, P. (1990). A model for the detection of motion over time, Proceedings of thr International Conference of Computer Vision, Osaka, Japan, 33-37.

Brox T., Bruhn A., Papenberg N., and Weickert J. (2004). High accuracy optical flow estimation based on a theory for warping. Proc. 8th European Conference on Computer Vision, 3024:25–36.

Brox T. and Malik J. (2010). Large displacement optical flow: descriptor matching in variational motion estimation. IEEE Trans. PAMI, 500-513.

Cetin, B., Dayioglu, A.Y., and Aydilek, A.H., 2016, Comparative Evaluation of Optical Flow Techniques to Define Strain Distribution in Geosynthetics, GeoAmericas 3rd Pan-American Conference on Geosynthetics, April 10-13, Miami Beach, US, 2:1298-1307.

Guler, M. Kutay, M.E., Aydilek, A.H., and Dafla, H. (2005). Evaluation of Strain Distribution in Geotextiles Using Image Analysis, *Proceedings of Geo-Frontiers 2005*, Austin, Texas, January 2005, 8 p.

Horn, B.K.P., and Schunck, B.G. (1981). Determining optical flow. Artificial Intelligence, 17, 185–203.

Kutay, M.E., Guler, M., Aydilek, A.H. (2006). Analysis of factors affecting strain distributions in geosynthetics, *Journal of Geotechnical and Geoenvironmental Engineering*, 132 (1):1-11.

Lucas B. and Kanade T.(1984). An iterative image registration technique with an application to stereo vision. DARPA Image Understanding Workshop, USA, 121–130.

Shinoda, M., and Bathurst, R. J. (2004). Lateral and axial deformation of PP, HDPE, and PET geogrids under tensile load. *Geotextiles and Geomembranes*, 22(4): 205–222.

Sun, D., Roth, S., and Black, M. (2010). Secrets of optical flow estimation and their principles. In IEEE Conference on CVPR, 2432–2439.